GEOLOGICAL SURVEY OF CANADA

OPEN FILE 2089

LITHOSTRUCTURAL MAP OF THE THOMPSON OPEN PIT THOMPSON NICKEL BELT, MANITOBA SCALE 1:1200 (1 INCH = 100 FEET)

W. Bleeker

1989

Energy, Mines and Resources Canada

Énergie, Mines et Ressources Canada

Canada

Manitoba
Energy and Mines

Contribution to Canada-Manitoba Mineral Development Agreement 1984-89, a subsidiary agreement under the Economic and Regional Development Agreement. Project funded by the Geological Survey of Canada.

Energy, Mines and Resources Canada

Énergie, Mines et Ressources Canada

GEOLOGICAL SURVEY OF CANADA

OPEN FILE 2089

LITHOSTRUCTURAL MAP OF THE THOMPSON OPEN PIT THOMPSON NICKEL BELT, MANITOBA SCALE 1:1200 (1 INCH = 100 FEET)[1]

W. Bleeker

LITHO-STRUCTURAL MAP OF THE THOMPSON OPEN PIT

THOMPSON NICKEL BELT, MANITOBA

SCALE 1 : 1200 (1 INCH : 100 FEET)

W. Bleeker

Department of Geology

University of New Brunswick

Fredericton, N.B. E3B 5A3

INTRODUCTION

Inco's Thompson Open Pit (TOP; Fig. 1) was mapped and sampled during the 1986 and 1987 field seasons as part of a Ph.D. study on the structure, metamorphism, setting and genesis of the Thompson Ni-sulphide ore body. Objectives of the mapping were to document the unique but temporary exposures of massive Ni-sulphides and enclosing host rocks, and to prepare a detailed geological base map to support further thematic studies. Within the limitations of time and exposure, mapping was focussed on lithological, structural, and metamorphic features, ore types, and ore-host rock relationships.

The more than 1500 m long TOP was designed to mine 6.5 million tons of Ni sulphide ore (Hopkins, 1986) that remained as crown pillars between 400' level underground operations and the surface. To get access to these near-surface ore reserves, extensive post-glacial overburden consisting mainly of varved clays had to be removed. This was accomplished by dredging during the period 1981-1986. Caprock drilling and first blasting of ore and wall rock commenced in early 1986.

Some bedrock exposure at the southwest end of the pit had been removed prior to initiation of this study. In this area, the map is based on remaining outcrops and surface projection of the geology exposed in the first benches, and is augmented in some areas by information from Inco's geological maps.

Low altitude 1:1200 (1 inch : 100 feet) aerial photographs were used as base maps. Due to considerable relief in the bedrock surface, the photographs introduced some distortion, but this was partly corrected by tying the mapping to Inco's "geology points" that were surveyed into the Thompson Mine grid. Remaining distortions may be as large as several mm on the map, but are gradual in nature and do not seriously affect the representation of geological relationships. In its present version, the map is primarily a base map for further detailed studies by the author, and thus shows some information, e.g. localities of samples, that is of little interest to others.

GENERAL OUTLINE OF THE THOMPSON STRUCTURE

The Thompson ore body is a stratabound deposit and occurs as a series of semicontinuous lenses within a biotite schist unit in a highly deformed Early Proterozoic supracrustal sequence known as the Ospwagan Group (Zurbrigg, 1963; Peredery, 1982; Bleeker, 1988; Bleeker and Macek, 1988) in the Thompson Nickel Belt (TNB; Fig. 1). The Ospwagan Group (Scoates et al., 1977; Bleeker and Macek, 1988) forms a thin but lithologically varied cover sequence, unconformably overlying Archean basement of the Superior Province.

During an early phase of the Hudsonian orogeny, basement and cover were deformed into a regional fold nappe (F_1; Bleeker, in press; Bleeker and Macek, 1988). The Thompson ore body occurs on the extremely deformed, overturned short limb of this regional recumbent fold, which probably verges towards the south. The mine

sequence is thus downward facing, with reworked basement overlying the strongly deformed cover rocks. This basement/cover relationship has been preserved in spite of intense superimposed deformation.

Most conspicuous among the younger structures, both on a mesoscopic and regional scale, are nearly upright, doubly-plunging F_3 antiforms and synforms which alternate in an échelon fashion. On the scale of the Thompson Nickel Belt, these F_3 folds form a left-stepping en échelon pattern, oblique to and 10-20° clockwise from the N35E trend of the belt. The pattern is the result of sinistral ductile wrenching of the F_1-F_2 nappe pile (Bleeker, in press). The Thompson Mine area is characterized by several of these NE trending F_3 antiforms and synforms. The mine sequence forms two regional scale doubly-plunging F_3 antiforms. Figure 2 shows a sketch of the Thompson structure and illustrates the location of the TOP on the southeast limb of the larger F_3 antiform, between the T1 and T3 shafts which provide access to the underground workings. The two main ore lenses that occur within the TOP, known as the 1B and 1C ore bodies are also shown in Figure 2.

In spite of intense polyphase internal folding, the supracrustal sequence preserves an overall northwesterly facing direction within the TOP (Bleeker and Macek, 1988). Lithological layering and layer-parallel S_1 and S_2 foliations from a composite transposition foliation which generally dips steeply to the SE. The hanging wall to the ore zone is thus formed by the stratigraphic footwall. Since small scale younging criteria are not preserved, only an overall younging direction can be defined based on a careful lithostratigraphic analysis of numerous localities in the Pipe II-Thompson region (Bleeker and Macek, 1988). Given the nature of the transposition foliation, the concept of lithostratigraphic younging breaks down on outcrop scale and can only be used in areas of good structural and lithostratigraphic control.

LITHOLOGIES

In this section, the lithologies exposed in the TOP are briefly described and indicated in the legend of the map. Where appropriate, local mine terms for the different lithologies are given in quotes.

Reworked Archean basement

1a) **Heterogeneous biotite gneiss**, locally with garnet and/or sillimanite; rare calc-silicate rich bands.

Medium grained biotite gneiss is dark grey and possesses a distinct gneissic layering. In the TOP, these gneisses are subordinate to granitoid gneisses and occur as irregular bands. No attempt has been made to map the commonly gradational contacts between the two gneisses. Bands (0.1-1.0 m) of coarse grained, diopside-rich calc-silicate gneiss containing minor disseminated pyrhotite were observed in several localities. This lithology can easily be confused with the calc-silicate gneisses ("skarns") of the cover sequence if encountered out of context, e..g. in drill core.

1b) **Amphibolite; disrupted mafic bodies.** Irregular bands, boudins or enclaves of medium to coarse grained amphibolitic gneiss, locally with garnet porphyroblasts can be confused with Proterozoic amphibolites (unit 10a), however, the Archean amphibolites/amphibolitic gneisses are generally coarser grained, more varied in texture, and commonly show more complex structure.

1c) **Granitoid gneiss.** Coarse grained, pink to grey, commonly strongly migmatitic gneiss of tonalitic to granodioritic bulk composition containing several generations of quartzofeldspathic neosomes is the dominant type of

gneiss. The lithology displays progressive grain size reduction toward the contact with the Ospwagan Group supracrustals.

The basement gneisses are well exposed in two shoulders on the southeast end and the northeast end of the TOP. In the latter locality, the overturned contact with quartzites of the cover sequence is preserved and should become progressively better exposed as more clay washes away. The contact is rather sharp, although locally obscured by conformable pegmatites, and is parallel to the gneissic layering in the reworked basement and the transposition layering in the supracrustals. Consequently its original nature should be interpreted with caution. However, the discovery of a basal quartz pebble conglomerate outside the TOP area, and the fact that in many widely separated localities, a closely similar lithostratigraphic sequence is observed in the supracrustals adjacent to this contact indicates that it can be interpreted as a tectonically modified unconformity.

Early Proterozoic lithologies: supracrustals and rocks of the ore zone

2. **Laminated feldspathic quartzite ("hangingwall quartzite").** The quartzites are grey-brown, light grey or white and are commonly laminated. A thin basal quartz pebble conglomerate has been discovered in several localities outside the Thompson Mine area. The quartzites (1-5 m thick within the TOP) contain up to 50 modal % feldspar, mainly microcline with lesser plagioclase, and 5-10% biotite. Locally sillimanite and retrograde muscovite after sillimanite are present in small amounts. The unit correlates with basal quartzites found in Manasan Quarry (used as a flux), Pipe II Open Pit, and along the west shore of Ospwagan Lake and the east shore of Mystery lake (visible prior to flooding).

3. **Veined biotite gneiss.** Biotite gneisse is a 1-5 m thick unit with abundant pink quartzofeldspathic "sweats". At lower metamorphic grade, this unit is a 5-20 m thick biotite schist with a typical dark mauve tint and pink "sweats". The gneissic appearance of this unit has resulted in its being confused with basement gneisses and this excellent marker horizon has therefore never been properly recognized. It was probably a psammitic wacke in origin. The unit generally lacks aluminous porphyroblasts, although a few rare garnet and sillimanite porphyroblasts have been observed in the TOP. Relict bedding is completely obliterated in the Thompson area but is present at the Pipe II Open Pit, Manasan Quarry and the west shore of Ospwagan Lake. Together with the basal conglomerate, quartzites, and overlying chemical sediments, this unit forms part of an originally transgressive fining upward sequence. This stratigraphic sequence, together with its unconformable relationship relative to adjacent gneisses, constitutes the best indicator of stratigraphic facing.

4a. **Calc-silicate gneiss.** Together with unit 4c, these rocks are locally known as "skarns". Their mineralogy consists of varying proportions of microcline, diopside, hornblende and actinolite, biotite, calcite, plagioclase, scapolite, quartz, grossular, epidote, sphene, opaque minerals and accessories such as small rounded grains of monazite. Some of these phases are retrograde in origin. These rocks generally exhibit thin compositional layering produced by differing mineral abundances. In some bands, a high mica content gives the rock a schistose character, whereas other bands consist of massive diopside.

They probably represent original impure chemical sediments with end members ranging from chert, siliceous dolomite, limestone, sulphide-rich laminae, to marls with an argillaceous clastic component.

4b. **Biotite gneiss intercalation.** A distinct 1 m wide band of veined biotite gneiss within unit 4 can be traced through much of the TOP.

4c. **Forsterite-diopside-phlogopite marble.** Marble is white to light green, with abundant porphyroblasts of forsterite and diopside. Forsterite is commonly serpentinized and diopside is commonly altered to tremolitic amphibole. Phlogopitic mica is common in the carbonate rich matrix. The rock can be massive or may show irregular compositional banding. Near its contacts, massive diopside bands and pinkish, fine grained siliceous layers are intercalated.

5. **Garnet-sillimanite-K-feldspar biotite schist.** These "biotite schists", are much more heterogeneous than previously described (e.g. Peredery, 1982). Besides the high grade pelitic schist with porphyroblasts of sillimanite, garnet and K-feldspar, and rare armoured relics of staurolite, the following lithologies occur as minor bands in this unit:

   1) **Highly graphitic schist** with significant pyrrhotite concentrations. Pyrrhotite forms thin laminae or schlieren, but may locally form up to 25 cm wide massive sulphide bands. This subunit occurs along the stratigraphic base of the schists and is overlain by:

   2) A 10-50 cm thick **silicate facies, banded iron formation** (indicated as --IF-- on the map). The couplet of sulphide-rich graphitic schist and silicate facies iron formation between the pelitic schists proper and the carbonate rich unit can be directly correlated with a similar lithological sequence at Pipe II Open Pit (Bleeker and Macek, 1988).

   3) **Thin siliceous layers with up to 50 modal % fine grained garnet.**

4) Several other layers of **chert-banded, silicate facies iron formation** and **highly graphitic schists with massive pyrrhotite bands up to 1 m** thick near the top of unit 5. The latter can be classified as sulphide facies iron-formation.

Ni-poor pyrrhotite in these "biotite schists" (unit 6c) is especially prominent at the northern end of the TOP, where the nickeliferous ore zone pinches out. Where the ore zone widens, distinction between the two types of sulphide becomes difficult, although inclusions, fragments, or bands of graphitic Ni-poor sulphides have been recognized within the 1B and 1C ore bodies. On a weathered surface, the two sulphide types are difficult to distinguish although the Ni-rich sulphides may be recognized indirectly by their ultramafic inclusions. The sulphides of "sedimentary" affiliation are very graphitic and poor in Ni, but Ni tenor appear to increase in proximity to massive nickeliferous sulphides. The presence or absence of pentlandite is thus not a reliable discriminator between the two sulphide types. Similar relationships have been described for the Ni ore and associated sulphidic sediments at Kambalda (Paterson et al., 1984).

6a. **Massive sulphide ore.** Massive, high grade, inclusion-poor sulphide ore contains abundant pentlandite porphyroblasts up to 2 cm in size. Of the relatively few inclusions or fragments of silicate rocks, ultramafic inclusions predominate. These ultramafic masses (= unit 7a) vary in size from 5 cm to larger than 100 m and consist generally of serpentinized dunites.

6b. **Inclusion-rich breccia ore.** Similar to and gradational with unit 6a but with progressively more wall rock inclusions, the breccia ore contains relatively fewer ultramafic inclusions, i.e. the original population of ultramafic inclusions has been diluted by progressively more wall rock inclusions. Except for the

ultramafic inclusions, all silicate rock inclusions in the breccia ore correspond to known adjacent wall rocks. It can be shown that many of the inclusions have been incorporated at a very late retrograde stage in the structural-metamorphic history, when much of the wall rock behaved in essentially brittle, fashion giving rise to a typical "Durchbewegung" structure (a sulphide mélange).

6c. **Minor, discontinuous sulphide stringers.** This unit includes the graphitic, Ni-poor sedimentary sulphide bands, in so far as they have been recognized. Where the ore zone widens, sedimentary sulphides could not be recognized in the rusty or dust covered outcrops, however, they could be identified in freshly broken ore after blasting. Where several sulphide bands occur close together, intercalated schist bands may be broken up into randomly oriented inclusions and the sedimentary sulphides become indistinguishable from minor stringers of unit 6b.

7a. **Serpentinized peridotite with net-textured interstitial sulphides.** Ultramafic boudins of variable size are distributed along the ore zone. The largest body occurs between the 1B and 1C ore bodies, whereas smaller boudins (1-10 m) occur as inclusions in massive sulphide ore (6a), especially at the south end of the TOP. Large ultramafic inclusions are rare along the 1C ore zone, except for two strongly altered bodies. However, many 5-50 cm size ultramafic inclusions were observed in the 1C breccia ore. The bodies are completely serpentinized and generally show progressive development of monomineralic, concentric metasomatic shells parallel to their contacts. A typical zonation consists of biotite, anthophyllite and talc zones surrounding the internal serpentinite core. Cumulate textures with interstitial sulphides are commonly preserved, in spite of complete serpentinization.

7b. **Ultramafite, unspecified**, apart from the ultramafic boudins scattered along the ore zone, a thin layer of completely serpentinized, ultramafic rock, occurs in the footwall of the ore zone, and is stratigraphically directly overlain by silicate facies iron formation.

8a. **Silicate facies iron formation.** One to several 0.1-10 m thick bands of chert-banded silicate facies iron formation form the most distinctive lithology in the footwall of the ore zone. Their mineralogy consists of garnet, grunerite, orthopyroxene, biotite, magnetite and minor sulphides, in addition to the quartz bands. Apatite-rich bands occur as intercalations.

8b. **Metachert**, Metachert consists of massive white quartz with minor pink garnets. Up to 1 m thick bands occur associated with the iron formations of unit 8a.

9. **Feldspathic quartzites with intercalated schists.** Although unit 8a forms the most distinctive marker in the footwall of the ore zone (stratigraphic hangingwall), a package of thinly banded quartzites with minor intercalated schists forms the footwall to either the ore zone or the schists of unit 5. These "footwall quartzites" grade into iron formation through several similar but distinctive cycles which consist of quartzite, minor silicate facies iron formation and massive white chert. In addition, thin bands (0.5-1.0 m) of dark green mafic schist occur as typical intercalations in this package. The quartzites are feldspathic, and contain minor biotite, sillimanite and/or garnet. Very similar quartzites with intercalated schists stratigraphically overlie the iron formations and form the northwest shoulder of the TOP and the core of the Thompson structure (hence the term "core quartzites"). These two quartzite-dominated units are lumped together as unit 9 on the map. The exact nature of these quartzites is not clear at present.

Early Proterozoic lithologies: infracrustals

10a. **Amphibolite; unspecified.** Lenticular bodies of amphibolite are common throughout much of the TOP, and are not necessarily all of the same type. The bodies have high aspect ratios and some appear to transgress the tectonostratigraphy at a low angle. The majority of these bodies is therefore interpreted as metamorphosed mafic dikes and tentatively correlated with the 1883 Ma Molson dyke swarm (Heaman et al., 1986). A supracrustal origin cannot be excluded for some of the amphibolites however.

10b. **Mafic schists.** Thin bands of grey-green to dark green mafic schists are intercalated in the "footwall quartzites". Some of these bands are of sufficient thickness to be mapped separately. Some of these schists may represent retrograded amphibolites. This lithology also occurs as rare inclusions in the breccia ore.

11. **Bronzite-forsterite porphyroblastic ultramafite.** This lithology ("ultramafic amphibolite") forms a large tabular body in the hangingwall of the TOP. It appears to occur in en échelon segments and to transgress the basement-metasediment contact. Although deformed, the body appears relatively coherent compared to the ultramafic boudins of the ore zone. All these characteristics, together with its composition, suggest that this body is part of an ultramafic Molson dyke, since the Molson dyke swarm is probably post-F1 in age (Bleeker and Macek, 1988). The rock consists of amphibole with interstitial green spinel, overgrown by large bronzite poikiloblasts and forsterite porphyroblasts. Towards its margins, the ultramafite becomes more schistose and grades into an amphibole-mica schist.

12. **Pegmatites.** Abundant pegmatites and finer grained granitic dikes and sills occur within the TOP. They can be classified structurally into several age

groups, e.g. syn-F2, syn-F3, post-F3. Several of the structurally better constrained pegmatites are being dated by the U/Pb-zircon and monazite method to date or bracket the various deformation phases.

13. **White vein quartz.** Large volumes of white vein quartz are associated with zones of brecciation at several places along the ore zone. Several phases of brecciation appear to overprint each other. Early brecciation is associated with pervasive retrogression in the pelitic schist, which is locally transformed into chlorite-sericite schist. Where the brecciation and quartz infilling interacted with the ore zone, complex "stockworks" of quartz and sulphide veins were formed. In proximity to these zones, lumps of white vein quartz, of variable size and roundness, are a dominant inclusion type in the breccia ore. The last phase forms relatively open fractures lined with clear quartz crystals, carbonate, marcasite and locally delicate millerite aggregates.

DEFORMATIONAL HISTORY

For a general overview of the tectono-metamorphic history of the Thompson Nickel Belt, the reader is referred to Bleeker (1988). A brief summary of the deformational history is given below, as background for the structural information given on the map and the accompanying orientation diagrams.

Earliest structures due to compressional tectonism are isoclinal F_1 folds such as the nappe-like structure that dominates the Thompson Mine-Pipe II Mine region. The Thompson Mine area is situated on the short, overturned and most highly strained limb of this structure. The metamorphic regime during F_1 is unknown but basement involvement in the nappe structures suggests at least lower amphibolite facies conditions. Timing of F_1 is uncertain but probably predates 1883 Ma since F_1 folds are cross-cut by mafic dykes which can be correlated with the Molson dyke swarm. F_1 is overprinted by a second phase of tight to isoclinal folding (F_2) which

developed under near-peak metamorphic conditions. On a mesoscopic scale F_2 folds are prominent and fold the Molson-like mafic dykes. Their macroscopic effect on the geometry is not yet fully understood, but they probably developed as recumbent folds.

The thermal peak of regional metamorphism outlasted F_2 and probably occurred between 1822 and 1800 Ma (N. Machado, pers. comm; Bleeker in press). The combined F_1-F_2 history can be interpreted as a phase of crustal thickening during which a SE tapering wedge of recumbent folds and thrusts was emplaced on the margin of the Superior plate. Thermal relaxation of the thickened crust culminated in the generation of anatectic granites and the thermal peak of metamorphism. At least 30 Ma later and at much lower temperatures, intense deformation attributed to sinistral wrenching of the recumbent fold pile produced the high amplitude, nearly upright, doubly-plunging F_3 folds, such as the Thompson structure (Fig. 2). These are the most obvious structures throughout the TNB, transposing the preexisting recumbent fold pile into a steeply dipping gneiss and schist belt.

Within the Thompson Mine area, F_3 folds are overprinted by open F_4 folds with shallowly dipping axial planes and shallowly ENE plunging axes. These folds are especially prominent in the southwest wall of the TOP. F_3 folds are overprinted by steeply plunging folds which classified as F_5. The age relationship between F_4 and F_5 is not yet established.

A phase of mylonitization overprints F_3 and is confined to shear zones which tend to be parallel to the steeply dipping limbs of the upright F_3 folds. Obvious kinematic indicators in these shear zones reveal dip-slip movement. These ductile shear zones are overprinted by pseudotachylite generating brittle-ductile and brittle faults, which are steep and (sub)parallel to the belt. These faults are concentrated along the western margin of the belt, and are especially numerous along the "Churchill-Superior boundary fault". Earlier faults indicate sinistral strike-slip displacement,

however, the last generation of pseudotachylites is generated along throughgoing dextral faults. A last generation of transcurrent faults forms a conjugate system at high angles to the belt, and is characterized by calcite-cemented fault breccias. Dextral faults of this system trend between N60-110E, whereas sinistral faults trend between N150-190E.

ORIENTATION DIAGRAMS

Structural data gathered in and around the TOP are presented in 24 orientation diagrams. All diagrams employ an equal area, lower hemisphere projection and are oriented relative to the map. Diagrams in the top row (plot 1 to 9) illustrate synoptic data, whereas the other diagrams (plots 10 to 24) are for specific domains or localities within the TOP. In discussing orientation data, the attitudes of planar or linear elements are given according to the format "dip direction/dip" or "trend/plunge". For example, S3: 135/65 refers to an S3 plane with dip direction N135E and a dip of 65°.

Plot 1. All poles to the layer-parallel transposition foliation ($\pi S_{0,1,2}$) in the metasediments and the gneissic layering (πS_{gn}) in the gneisses (n = 427).

Note the non-cylindrical distribution of the poles to the main foliation. Two diffuse π-girdles can be defined with NE and SSW plunging π-girdle axes (c.f. plot 11), reflecting the doubly plunging nature of the dominant F_3 folds. The distribution reflects the similarity of the mesoscopic structures in the TOP and the overall macrostructure (Fig. 2), i.e. an illustration of "Pumpelly's rule". It is important to note that pole figures throughout the TNB define essentially similar distributions, illustrating the homogeneity of the TNB with respect to F_3 structures.

Plot 2. All linear structures in the TOP (small open circles, n = 299), compared with macroscopic F_3 axes of the main antiformal hinge at the T1 underground mine (cluster of 5 large solid dots marked by "T"), macroscopic F_3 axis of the Pipe Mine fold (large solid dot marked "P", macroscopic F_3 axis of the Manasan Quarry fold (large solid dot marked "M"), and mesoscopic F_3 axes measured at Pipe II Open Pit and Manasan Quarry (small solid dots, n = 16).

Note that all linear structures define a great-circle girdle, including the Pipe Mine and Manasan Quarry data, with estimated orientation 135/65. Similar girdles are characteristic for all of the TNB (Bleeker, 1988) and represent the axial planes of F_3 macrostructures (S_3). F_3 doubly plunging axes are of course confined to this S_3 girdle, whereas all pre-F_3 fold axes were rotated towards this girdle due to the tight nature of F_3 macrostructures. Post-F_3 linear structures will in general be constrained by the limbs of the tight F_3 folds and therefore also plot on or close to this girdle.

Plot 3. All F_3 related linear structures from the TOP, i.e. mesoscopic F_3 axes (small open circles, n = 180) and related crenulation or intersection lineations (small solid dots, n = 28). The macroscopic axes of the T1 antiformal hinge are given for reference (large solid dots, n = 5). The diagram also shows measurements of a single non-cylindrical axis of a strongly doubly plunging F_3 fold (large open circles, n = 5; locality 3, 29300N-9400E).

All linear F_3 structures (B_3 and L_3) define the S_3 girdle described in plot 2. Note that S- and Z-asymmetric F_3 folds plot in two distinct fields, consistent with the position of the TOP on the SE limb of a macroscopic doubly plunging antiform. The strong separation of the two groups along the girdle reflects the "mildly" doubly plunging nature of the Thompson structure, whereas elsewhere in the TNB

continuous girdles without a central gap suggest progressive rotation towards sheath-like structures. Such sheath-like F_3 folds are indeed observed on a mesoscopic scale. Note also that the macroscopic F_3 axes for the T1 antiformal hinge plunge steeper than the average of Z-asymmetric F_3 axes in the TOP, compatible with the position of the TOP closer to the culmination of the Thompson structure.

Plot 4. All pre-F_3 linear structures from the TOP, i.e. F_1 fold axes (solid squares, n = 2), F_2 fold axes (open squares, n = 37), amphibole mineral lineations (L_a, n = 10) and other L_2 lineations (mostly S_1/S_2 intersection lineations; L, n = 17).

Note refolding of a single F_2 axis (large open squares) by a local F_3 axis (open circle), i.e. they plot on a small circle around the latter axis (dash-dot line). This explains much of the spread across the S_3 girdle. The spread along the S_3 girdle either indicates an initial non-cylindrical nature of F_2, or rotation related to the non-cylindrical nature of F_3, or both. Amphibole mineral lineations are in general parallel to nearby F_2 axes.

Plot 5. Structural data on the mylonite exposure along the highway in Thompson. Shown are the average attitude of the foliation in the mylonitic gneisses (dashed great circle), axes of vertical sheath folds (small open circles, n = 7) and associated stretching lineations (small solid dots, n = 4).

This outcrop of (proto) mylonitic gneisses forms part of the Burntwood River Lineament, one of the main mylonitic fault zones subparallel to the TNB. Kinematic indicators reveal dip-slip with SE side up, NW side down. The same movement is thought to have contributed to steepening of F_3 fold axes of the Thompson structure.

Plot 6. Additional data on the mylonite outcrop of plot 5. The data in this diagram relate to structures that overprint the mylonitic foliation, i.e. late vertical S-asymmetric folds and pseudotachylite generating minor brittle faults. Indicated are axes of the late asymmetric folds (small open circles, n = 3), poles to the mylonitic foliation around this fold (small solid dots, n = 11), associated π-girdle and its axis (open circle with cross). The pseudotachylite generating faults are shown as the (sub)vertical dashed great circles. Where known, the sense of displacement is indicated.

The asymmetry of the vertical fold suggests late sinistral movement on the Burntwood lineament. F_5 folds, i.e. vertical folds superimposed on the Thompson structure are possibly related to these late folds in the mylonite zone. Displacements on the pseudotachylite-generating minor faults indicate sinistral offsets, and the pseudotachylites appear deformed and recrystallized. The N-trending orientation may correspond to an R-shear direction.

Plot 7. Poles to all joints measured in the TOP (n = 179).

Four major sets can be distinguished. Two vertical sets form a conjugate system of shear joints. A third set constitutes sub-horizontal joints (n = 28), whereas a fourth set is formed by joints dipping $\pm 50°$ (n = 23) in northerly directions. The latter set causes major stability problems for some of the walls in the TOP.

Plot 8 and 9. Orientation of the shear joint system in the TOP. Diagram 8 gives all poles to joints with sinistral shear displacement (n = 22) and a rose diagram of their trends. Diagram 9 gives similar data for the dextral set (n = 37).

Most of the vertical joints in the TOP appear to be associated with this system and typically form an échelon arrays. Their orientations appear to conform to R, T, R' and P orientations. The shear joints (minor faults) are often coated with calcite, locally accompanied by sulphides such as marcasite or pyrite. The joint planes intersect subvertically, and show horizontal slickensides striae. This system of shear joints (minor transcurrent faults) is related to a larger system of conjugate transcurrent faults which cut obliquely across the TOP. Individual shear joints show up to several meters of brittle offset of the ore zone. The same conjugate system of brittle transcurrent faults has been noted at Ospwagan Lake and in Pipe II Open Pit. The system indicates NW-SE compression, possibly related to residual convergence between the Superior plate and the Churchill Province.

Plot 10. Structural data for locality 72 (28975N-8850E). Open to tight F_3 folds in footwall quartzites (unit 9). Indicated are poles to the layer-parallel transposition foliation $\pi S_{0,1,2}$ (small solid dots, n = 16), the π-girdle through these poles (dashed great circle) and its π-girdle axis (open circle with cross), F_3 fold axes (small open circles, n = 6), and the S_3 axial plane (dash-dot great circle).

Plot 11 and 12. Structural data for localities 107 and 111, NW shoulder of 1C pit (e.g. 30500N-9200E). "Core quartzites" with abundant mafic boudins. Plot 11 indicates poles to the layer-parallel foliation $\pi S_{0,1,2}$ (small dots, n = 107). Plot 12 indicates mesoscopic F_3 fold axes (open and solid circles, n = 44).

Note the strong non-cylindrical overall distribution of the poles, reflecting the doubly plunging nature of the F_3 folds. Two π-girdles can be distinguished (dashed great circles in plot 11). Their axes (open circles with crosses) constrain the S_3 axial

plane (dash-dot great circle). Note the distribution of F_3 fold axes along this axial plane (open and solid circles, plot 12). Solid circles are axes of a single mesoscopic, strongly doubly plunging F_3 fold (n = 5).

Plot 13. Structural data for localities 18 to 23, schists and quartzites in hangingwall and footwall of 1C ore body (between 29900N-9500E and 30500N-9500E). Indicated are poles to the layer-parallel transposition foliation $\pi S_{0,1,2}$ (small solid dots, n = 43), F_3 fold axes (open circles, n = 47) and the average S_3 axial plane (dash-dot great circle).

Note again the doubly plunging nature of the F_3 folds, and their asymmetries.

Plot 14. Structural data for the open F_3 folds observed in the NW wall of the 1C pit. Indicated are poles to the $S_{0,1,2}$ transposition foliation (small dots, n = 15), the associated π-girdle (dashed great circle) and its axis (open circle with cross), and a measured F_3 axis (open circle, n = 1).

Plot 15. Structural data for localities 93, 130 and 131. Northeast end of 1C pit, between 30600N-9650E and 31300N-9600E. The diagram indicates poles to $S_{0,1,2}$ (small solid dots, n = 10), the associated π-girdle (dashed great circle) and its axis (open circle with cross), F_3 fold axes (open circles, n = 3) and the S_3 axial plane (dash-dot great circle).

Plot 16. Structural data for localities 3 to 17, hangingwall of 1C pit, between 29300N-9400E and 30100N-9600E. Indicated are poles to $S_{0,1,2}$ (small solid dots,

n = 38), F_3 fold axes (open circles, n = 10) and associated crenulation or intersection lineations (large solid dots, n = 7), F_2 fold axes (open squares, n = 7) and associated mineral lineations (L, n = 3).

Plot 17. Structural data for sheath-like folds in "hangingwall quartzites", locality 3 (29300N-9400E). Indicated are poles to $S_{0,1,2}$ (small dots, n = 13), the associated π-girdle (dashed great circle) and its axis (open circle with cross), F_3 fold axes (open circles, n = 13) including 5 axes measured at various locations on a single sheath-like fold (along the S_3 great circle), and associated lineations (large solid dots, n = 9).

The steeper lineations appear to be stretching lineations. Asymmetry of the sheath-like folds (in outcrop) indicates that the SE side moved up relative to the NW side, i.e. a similar movement sense to that indicated in the mylonite outcrop at Thompson.

Plot 18. Structural data for locality 23, hangingwall to 1C ore body (30200N-9550E). Indicated are poles to $S_{0,1,2}$ (small dots, n = 9), F_3 fold axis (open circle, n = 1), L_3 intersection lineation (large solid dot, n = 1), F_1 fold axis (solid square, n = 1), F_2 fold axes (open squares, n = 6). Part of a small circle around the F_3 axis is shown for reference.

Plot 19. Structural data for locality 22, schists in hangingwall to 1C ore body (30000N-9500E). Indicated are poles to $S_{0,1,2}$ (small dots, n = 6), F_3 fold axes (open circles, n = 14) and associated crenulation lineations (large solid dots, n = 3), and F_2 fold axes (open squares, n = 3).

Note again the asymmetric grouping of F_3 folds, and the refolding of the two F_2 axes around a particular F_3 axis indicated by B_3 in the diagram.

Plot 20. No data.

Plot 21. Structural data for southeastern gneiss shoulder and adjacent metasediments at the southwest end of the pit. Both gneisses and metasediments have been folded into a rather open, south plunging F_3 antiform/synform pair. This diagram gives the data for the metasediments, and should be compared with the data for the gneisses in plot 22. Indicated are poles to $S_{0,1,2}$ in the metasediments (small dots, n = 25), the associated π-girdle (dashed great circle) and its axis (open circle with cross), mesoscopic F_3 fold axes (open circles, n = 9), macroscopic F_3 axes from the main antiform at T1 (large solid dots, n = 5) and the S_3 axial plane (dash-dot great circle).

Plot 22. As plot 21, but data are for the gneisses. Indicated are poles to the gneissic layering (S_{gn}; small dots, n = 36), the associated π-girdle (dashed great circle) and its axis (open circle with cross), mesoscopic F_3 fold axes (open circles, n = 32), macroscopic F_3 fold axes from the main antiform at T1 (large solid dots, n = 5), and the S_3 axial plane (dash-dot great circle).

Note that the F_3 structure in the gneisses is identical to the F_3 structure in the adjacent metasediments. The gneissic transposition foliation in the reworked basement is thus structurally comparable with the $S_{0,1,2}$ transposition foliation in the metasediments. The two structural elements must have attained parallelism prior to F_3, probably during F_1 recumbent folding. Complete obliteration of the Archean basement structures, with the new gneissic layering being parallel to the modified unconformity, qualitatively indicates the very high strain associated with F_1.

Plot 23. The same domain as plots 21 and 22. β-diagram for associated S_{gn}-L_3 pairs. S_{gn} indicated by dashed great circles (n = 7), associated L_3 crenulation lineation as open circles. Again, indicated for comparison are the macroscopic F_3 axes for the main antiform at T1 (solid dots, n = 5).

The data indicate that the south plunging antiform-synform pair in the gneiss shoulder is of the same generation as the small scale F_3 folds. All these folds are parasitic to the main south plunging F_3 antiform at T1.

Plot 24. Structural data related to F_4 folds in metasediments at the southwest end of the TOP (e.g. 26250N-8500E). Indicated are poles to $S_{0,1,2}$ for this domain (small dots and crosses, n = 69), the associated F_3 π-girdle (dashed great circle), mesoscopic F_3 axes (open circles, n = 8) and related F_3 crenulation lineations (large solid dots, n = 7). Some of the poles (those indicated by +, n = 18) were measured on limbs of open F_4 folds. Associated F_4 axes (4, n = 7) plot within the field surrounded by the dotted line. F_4 axial planes are rather shallow dipping and show fanning (two measured axial planes are indicated by finely dashed great circles.

F_4 folds, conspicuous in the SW wall of the TOP, are only visible in sections. They probably caused much of the local steepening and flattening of the ore zone as observed in underground stopes. F_4 is probably related to partial collapse under gravity of the high structural relief formed by the nearly-upright, high amplitude F_3 folds.

ACKNOWLEDGMENTS

This research is part of a Ph.D. study support by the Geological Survey of Canada, and is a contribution to the Canada-Manitoba Mineral Development Agreement 1984-1989. The permission granted by Inco Limited providing access to mine workings, drill core and records, and to publish these results is gratefully acknowledged. Many individual Inco staff geologists, especially Gary Sörensen, are thanked for their support during the work at Thompson Open Pit. Discussions with Paul F. Williams improved the geological content of this report.

REFERENCES

Bleeker, W.

(in press): New structural-metamorphic constraints on Early Proterozoic oblique collision along the Thompson Nickel Belt, northern Manitoba, Canada; in The early Proterozoic Trans-Hudson Orogen, ed. J.F. Lewry and M.R. Stauffer, Geological Association of Canada, Special Paper.

Bleeker, W. and J.J. Macek

1988: Thompson Nickel Belt Project—Pipe Pit Mine; Report of Field Activities 1988, Manitoba Energy and Mines, p. 111-115.

Heaman, L.M., Machado, N., Krogh, T., and Weber, W.

1986: Precise U-Pb zircon ages for the Molson Dyke swarm and the Fox River sill: implications for Early Proterozoic crustal evolution in NE Manitoba, Canada; Contributions Mineralogy Petrology, v. 94, p. 82-89.

Hopkins, J.L.

1986: Live at twenty-five. Canadian Mining Journal, July 1986, p. 29-31.

Paterson, H.L., Donaldson, M.J., Smith, R.N., Lenard, M.F., Gresham, J.J., Boyack, D.J., and Keays, R.R.

1984: Nickeliferous sediments and sediment-associated nickel ores at Kambalda, Western Australia; in Sulphide deposits in mafic and ultramafic rocks, ed. D.L. Buchanan and M.L. Jones; The Institution of Mining and Metallurgy, p. 81-94.

Peredery, W.V. and Geological Staff

1982: Geology and nickel sulphide deposits of the Thompson belt, Manitoba; in Precambrian sulphide deposits, H.S. Robinson memorial volume, ed. Hutchinson, R.W., Spence, C.D., and Franklin, J.M.; Geological Association Canada, Special Paper 25, p. 165-209.

Scoates, R.F.J., Macek, J.J., and Russel, J.K.

1977: Thompson Nickel Belt project. In: Report of Field Activities. Manitoba, Mineral Resources Division, p. 47-53.

Zurbrigg, H.F.

1963: Thompson Mine geology. Canadian Institute Mining Metallurgy Bulletin, 56, p. 451-460.

FIGURE CAPTIONS

Figure 1. Simplified geological map of the northwestern corner of the Superior Province, the Thompson Nickel Belt (TNB) as part of the Churchill-Superior Boundary Zone, and the adjacent Churchill Province. Note the locations of Thompson and Pipe Mine.

Figure 2. Simplified sketch of the Thompson structure. The structure consists of two doubly plunging F_3 antiforms. The Thompson Open Pit is situated on the steeply SE dipping, southeasterly limb of the structure, between the T1 and T3 shafts. Two major ore lenses occur within the open pit, which are referred to as the 1B (the lens closest to T1) and 1C ore bodies.

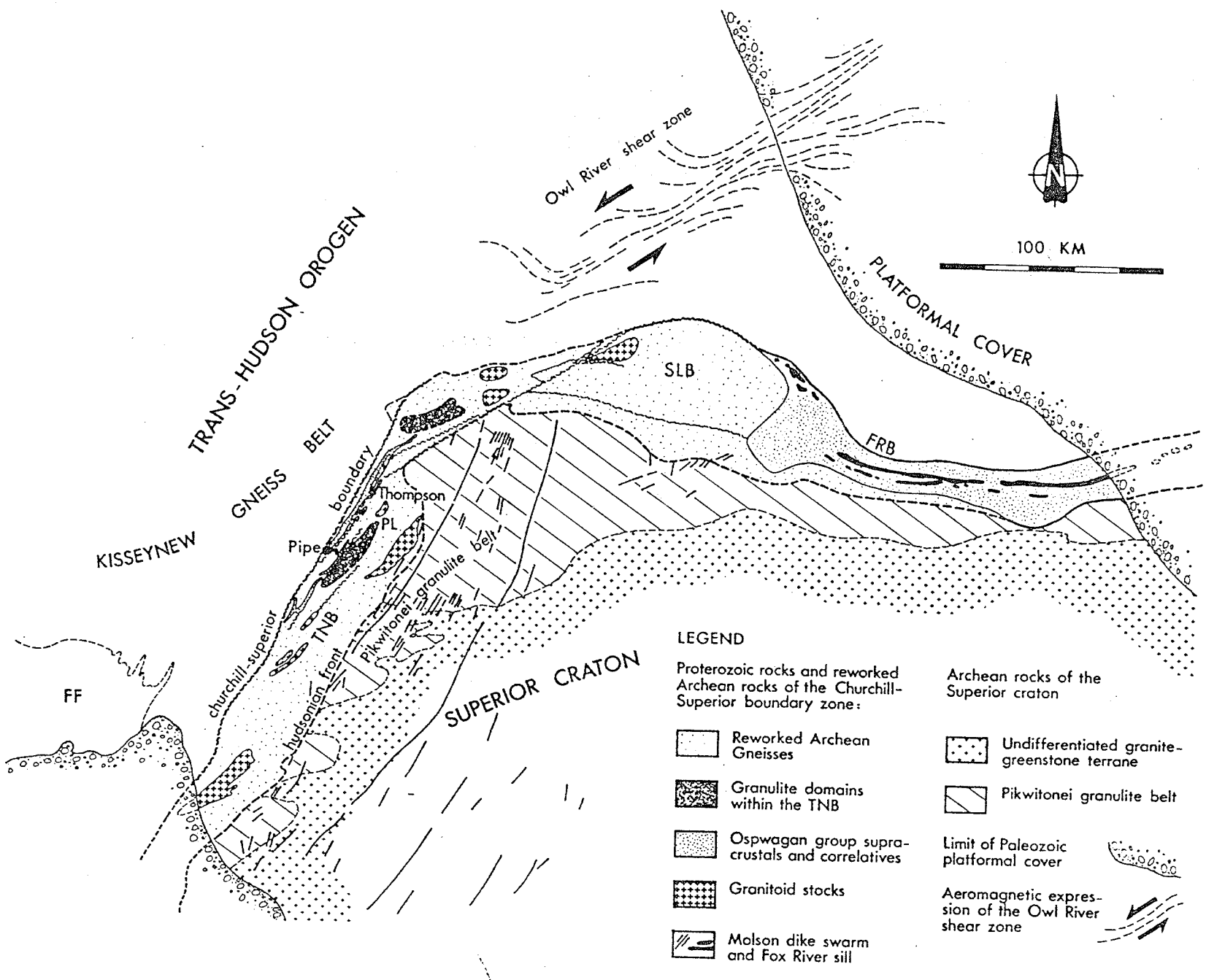
Owl River shear zone
TRANS-HUDSON OROGEN
GNEISS BELT
KISSEYNEW
PLATFORMAL COVER
100 KM
SLB
FRB
boundary
Thompson
PL
Pipe
belt
Pikwitonei granulite
churchill-superior
TNB
hudsonian front
FF
SUPERIOR CRATON
LEGEND
Proterozoic rocks and reworked Archean rocks of the Churchill-Superior boundary zone:
Reworked Archean Gneisses
Granulite domains within the TNB
Ospwagan group supra-crustals and correlatives
Granitoid stocks
Molson dike swarm and Fox River sill
Archean rocks of the Superior craton
Undifferentiated granite-greenstone terrane
Pikwitonei granulite belt
Limit of Paleozoic platformal cover
Aeromagnetic expression of the Owl River shear zone

Fig. 1

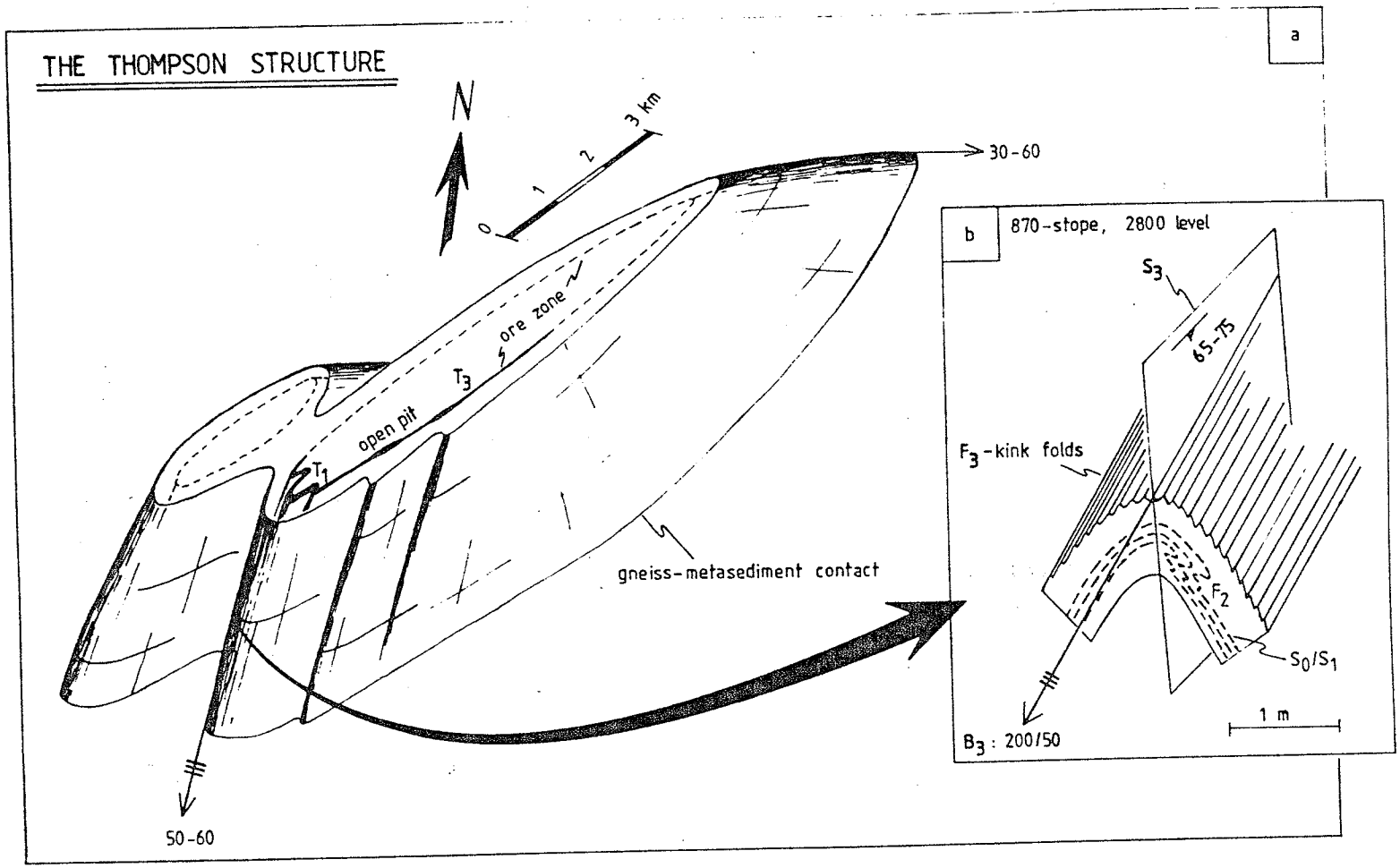
THE THOMPSON STRUCTURE
a
N
0
1
2
3 km
30-60
50-60
ore zone
open pit
T_3
T_1
gneiss-metasediment contact
b
870-stope, 2800 level
S_3
65-75
F_3-kink folds
F_2
S_0/S_1
1 m
B_3 : 200/50

Fig. 2